THE JOURNAL OF PHYSICAL CHEMISTRY C

Article

pubs.acs.org/JPCC

CO_2 Binding and Induced Structural Collapse of a Surface-Supported Metal–Organic Network

Jan Čechal,[*,†,‡] Christopher S. Kley,[†,◆] Rémi Pétuya,[§] Frank Schramm,[∥] Mario Ruben,[∥,⊥] Sebastian Stepanow,[*,†,#] Andres Arnau,[§,▽] and Klaus Kern[†,○]

[†]Max Planck Institute for Solid State Research, Heisenbergstrasse 1, 70569 Stuttgart, Germany

[‡]CEITEC and Institute of Physical Engineering, Brno University of Technology, Purkyňova 123, 612 00 Brno, Czech Republic

[§]Donostia International Physics Centre (DIPC), E-20018 Donostia - San Sebastián, Spain

[∥]Institute of Nanotechnology, Karlsruhe Institute of Technology, 76344 Eggenstein-Leopoldshafen, Germany

[⊥]IPCMS-CNRS UMR 7504, Université de Strasbourg, 23 Rue du Loess, 67034 Strasbourg, France

[#]ETH Zürich, Department of Materials, Hönggerbergring 64, 8093 Zürich, Switzerland

[▽]Departamento de Fisica de Materiales UPV/EHU and CFM-MPC Donostia, Centro Mixto CSIC-UPV/EHU, E-20018 Donostia - San Sebastián, Spain

[○]Institut de Physique de la Matière Condensée, Ecole Polytechnique Fédérale de Lausanne, 1015 Lausanne, Switzerland

Supporting Information

ABSTRACT: Extensive efforts have been directed toward identifying catalytic material composites for efficiently transforming CO_2 into valuable chemicals. Within this longstanding scientific challenge, the investigation of model systems is of particular interest to gain fundamental insight into the relevant processes and to synergistically advance materials functionalities. Inspired by the ubiquitous presence of metal–organic active sites in the conversion of CO_2, we study here the interaction of CO_2 with a two-dimensional metal–organic network synthesized directly on a metal surface as a model system for this class of compounds. The impact of individual CO_2 molecules is analyzed using scanning tunneling microscopy supported by density functional theory calculations. Dosage of CO_2 gas to the thermally robust Fe-carboxylate coordination structure at low temperatures (100 K) leads to a series of substantial rearrangements of the coordination motif, accompanied by a collapse of the entire network structure. Several binding sites of weak and moderate strengths are identified for CO_2 near the iron nodes leading to a moderate structural weakening of the existing coordination bonds in the adapted models with no indication of CO_2 dissociation. The observations suggest a concerted reaction pathway involving both CO_2 and ligand molecules starting at irregular coordination sites that may eventually lead to the collapse of the entire network structure. The electronic properties of the Fe atoms in the carboxylate environment are determinant for the response of the network toward CO_2, which depends critically on the local coordination environment. The results highlight that finely tuned metal–organic complexes and networks at surfaces present promising features to activate and transform CO_2.

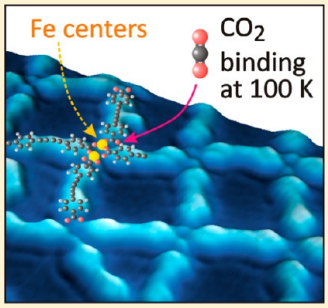

INTRODUCTION

Facing the steeply rising global energy demand and rapid depletion of fossil resources, novel concepts for sustainable energy conversion and storage, as well as alternative carbon sources for the synthesis of chemicals and fuels, are required.[1] Part of a greater comprehensive and multifaceted strategy to tackle this issue is the conversion of atmospheric CO_2 into high-energy density compounds. Significant research has been dedicated to capture and store CO_2, as well as utilize it as feedstock for chemical synthesis.[2−5] However, the selective transformation of CO_2 is highly challenging, requiring both appropriate catalysts and energy input. Currently, the technical reduction of CO_2 and/or its incorporation into organic molecules is prevalently mediated by homogeneous catalysts,[2−4] molecular[6] or enzymatic electrocatalysts,[7] as well as various other complex materials.[8,9] In this context, metal–organic frameworks have emerged as a promising class of porous materials[10−12] for gas storage[13−16] or catalysis,[17] combining the favorable characteristics of both heterogeneous and homogeneous catalysts, while only recently demonstrated as electrocatalysts for CO_2 reduction.[18] Likewise, surface-confined supramolecular architectures, i.e., metal–organic coordination networks (MOCNs), have attracted significant attention with potential applications in the areas of surface patterning, host guest chemistry, molecular electronics and spintronics.[19−21] MOCNs comprise individual and coordinatively unsaturated transition metal atoms or dimers that bear high potential for a new class of bioinspired catalysts.[22] The

Received: June 3, 2016
Revised: August 5, 2016
Published: August 5, 2016

DOI: 10.1021/acs.jpcc.6b05582
J. Phys. Chem. C 2016, 120, 18622−18630

first experiments demonstrated the catalytic action of the metal centers by the dissociation of O_2 through the concerted action of carboxylate bridged Fe^{2+} dimers[23] and by the electrochemically driven oxygen reduction or hydrogen evolution reaction.[24−26] It is, therefore, intriguing to explore the potential of these systems to fix, activate, and transform the chemically inert CO_2 molecule and to gain insight into the interaction of CO_2 with the system's components at the molecular level. In this respect, the interaction of CO_2 with open side positions at Au atoms covalently bound in Au-phenylene diisocyanide chains on gold surfaces was reported recently.[27,28]

Here, we report on the binding and reactivity of CO_2 with a model system comprising Fe centers embedded in a surface-confined MOCN at low temperatures of ∼105 K. The adsorption induced changes in morphology were followed by scanning tunneling microscopy (STM) at the single molecule level. The interpretation of the data was supported by first-principles density functional theory (DFT) calculations using a van der Waals functional with consistent treatment of exchange (vdW-DF-cx) and correlation.[29,30] Notably, despite the rather inert character of CO_2, our data reveal that individual CO_2 molecules readily interact with the MOCN components, resulting in substantial rearrangement of the network structure. Several binding modes and a potential mechanism for the induced disorder are discussed.

METHODS

Experimental Section. Experiments were carried out in an ultra-high-vacuum chamber (base pressure ∼ 2×10^{-8} Pa) hosting a homemade low-temperature scanning tunneling microscope operating at 5 K, and standard tools for surface preparation. Clean Ag(001) surfaces were obtained by repeated cycles of Ar^+ sputtering and annealing at 800 K, followed by a slow cooling to room temperature. The metal−organic networks were prepared by simultaneous deposition of Fe atoms and 4,4′-di(1,4-buta-1,3-diynyl)-benzoic acid (BDBA, Figure 1) molecules on the substrate held at 450 K.[31−33] BDBA

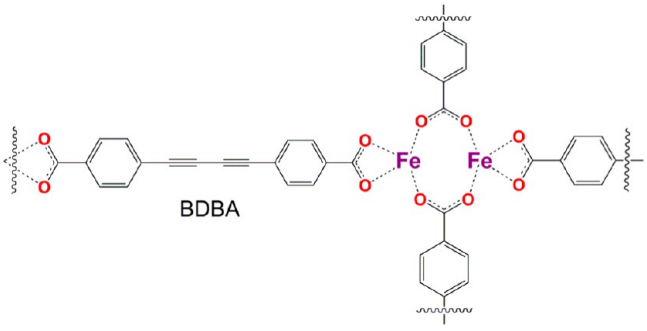

Figure 1. Chemical structure of the Fe-dimer node of Fe-BDBA 2D-MOCN.

was deposited by thermal evaporation from a quartz crucible at a temperature of 560 K. Fe atoms were deposited using a standard e-beam evaporator (Omicron EFM3) at a flux current of 1 nA. During the deposition (5−30 min), the pressure was lower than 2×10^{-7} Pa. Subsequently, the samples were transferred to the STM. STM images were acquired at 5 K using electrochemically etched tungsten or gold tips with a sample bias in the range from −1.4 to +1.0 V and tunneling currents ranging from 0.08 to 1.0 nA. For CO_2 dosing, the manipulator was precooled to 100 K (pressure ∼ 1×10^{-8} Pa); then the sample was inserted in the manipulator with time for thermal equilibration. CO_2 (purity 99.998%) was dosed at a partial pressure of 5×10^{-6} Pa (1 L) and 5×10^{-5} Pa (10, 100 L), respectively. The dose is given in langmuir (L); one langmuir corresponds to an exposure of 10^{-6} Torr during 1 s, i.e., 1 L = 1.44×10^{-4} Pa s. The purity of the dosed gas was checked in situ by mass spectrometry. For a detailed discussion on impurity analysis, see the Supporting Information (section 4). The mass filtered temperature induced desorption curves were obtained employing a Pfeifer mass spectrometer. For the measurements, the cold sample taken from the STM (5 K) was inserted into the precooled manipulator (105 K) and positioned in front of the mass spectrometer with its surface normal pointing directly into the center of the focusing ion optics. The sample was heated by a filament (current 4.5 A) positioned near the back side of the sample. The heating rate linearly decreased with increasing sample temperature from an initial value of 2.5 K/s (at 110 K) to 1 K/s (at 260 K). The position of the desorption peak was determined by fitting the curve by a third-order polynomial function after subtracting a linear background. The synthesis of BDBA is described in the Supporting Information of ref 31.

Computational Details. The DFT-vdW calculations were performed with VASP.[34,35] The Fe-BDBA coordination network on Ag(001) was modeled using a (8×6) ((8×8) for the Figure 7 I structure) Ag(001) single layer periodic supercell. BDBA ligands were limited to a benzene ring with a carboxylate substituent. The reduction of the system to individual Fe dimer centers with benzoate units on a single Ag layer representing the substrate introduces some approximations that are necessary to describe the system using ab initio DFT calculations. While the formation of bonds between CO_2 and Fe or carboxylic groups is still well described up to second nearest neighbors, the main drawback of such a model is the imposed geometrical constraint of rigidity in the Ag layer and the fact that only a part of the molecule is geometrically optimized. More precisely, we only relax the (x,y) coordinates of C and H atoms in the aromatic ring of the benzoate units, while all the (x,y,z) coordinates of the CO_2 molecule, O atoms in the carboxyl groups of the benzoate units, and Fe atoms are relaxed. As a consequence of these constraints, we cannot describe the influence of the structural changes at one coordination node to the neighboring ones. Whereas this model has certain limitations, it permits a good description of molecule−surface interactions in such a large system.[36] The projector augmented-wave (PAW) method[37] was used to describe the ion−electron interaction, whereas the exchange and correlation potential was taken into account by the generalized gradient approximation (GGA).[38] VdW dispersion forces were included using the vdW-DF-cx method.[29,30] An energy cutoff of 500 eV was employed for the plane-wave expansion, as well as a k-points mesh of 2×3 in the 1×1 unit cell to sample the Brillouin zone in the reciprocal space. For all calculations, the electronic convergence criterion was 1×10^{-4} eV, while the convergence on forces in the relaxation was 0.5 eV/nm. In any case, after testing the ligands adsorption distance, the acene rings vertical position was kept fixed (relaxation only in X and Y), at z = 0.30 nm for the 2b structure, during geometrical optimizations. All other atoms were relaxed in X, Y, and Z. STM simulations were done in the Tersoff−Hamann approximation.[39]

DOI: 10.1021/acs.jpcc.6b05582
J. Phys. Chem. C 2016, 120, 18622−18630

RESULTS AND DISCUSSION

The regular arrays of unsaturated coordination centers (see Figure 2a) were prepared by well-established codeposition of BDBA and Fe atoms on a Ag(001) surface under ultra-high-vacuum conditions.[31−33] The regular unperturbed coordination nodes of the MOCN consist of dimeric μ^2-carboxylate bridged Fe centers axially coordinated by bidentate chelating carboxylate moieties (Figure 1). Each Fe center adopts a distorted square planar coordination geometry.[23,31,40] The network components feature a high degree of adaptability, in particular, of the orientation of the ligand molecules and of the coordination geometry, which is manifested by the observation of monodentate axial carboxylate binding and other irregular low symmetry or distorted network nodes (see Figure 2a). Despite the absence of strict periodicity, the network grows continuously over the substrate area.[31] The MOCN is further characterized by an appreciable temperature stability up to 490 K beyond which the ligand molecule decomposes. A necessary starting point for the theoretical analysis of the CO_2 modified structures is the optimization of the core Fe dimeric coordination structure on the surface by DFT calculations. Figure 2b,c shows the reduced models for the most frequent coordination geometries inferred from the experimental data (see the Supporting Information, section 6, for details). The theoretical molecular appearances obtained in the Tersoff−Hamann approximation (Figure 2d,e) are consistent with the experimental STM images and confirm the adapted coordination motifs.

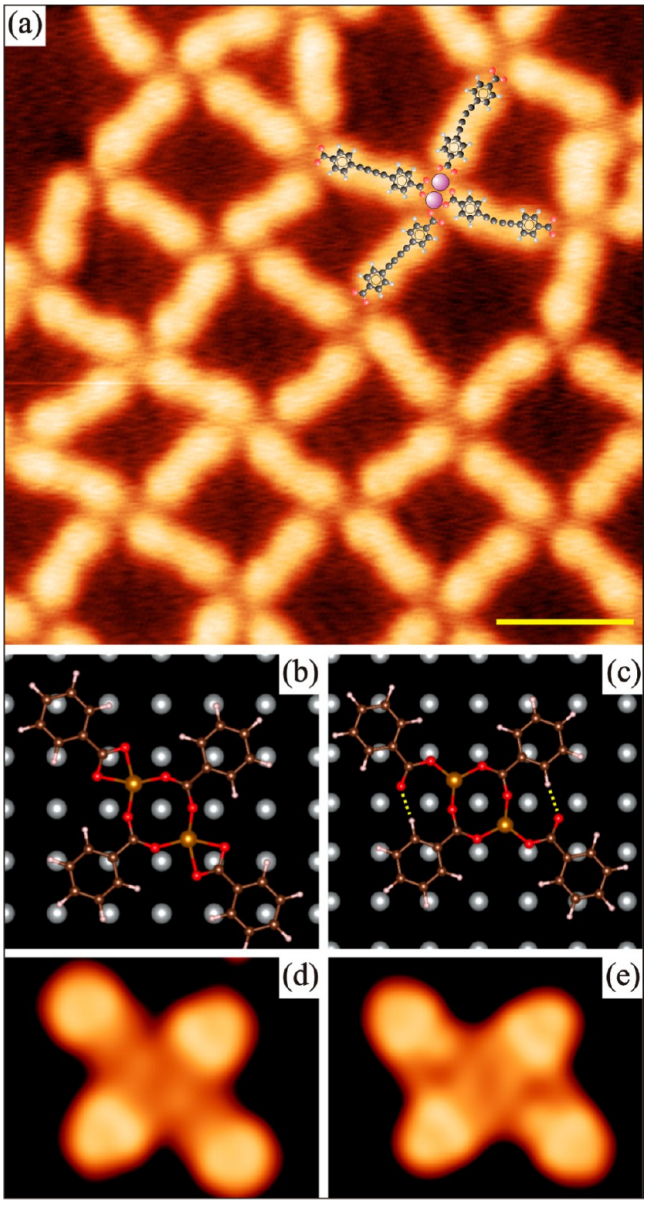

Figure 2. (a) Representative STM images of the pristine Fe-BDBA coordination network on Ag(001) imaged at 5 K. (b, c) Ball-and-stick models of the two optimized equilibrium structures of the pristine coordination nodes from DFT calculations with their (d, e) corresponding (Tersoff−Hamann[45]) simulated STM appearances. Yellow dashed lines represent hydrogen bonds (see the Supporting Information, section 6, for details). Acquisition parameters: −0.8 V, 0.5 nA. Scale bar: 2 nm.

Dosing of 100 langmuir (L) of CO_2 gas at a sample temperature of 105 K results in substantial structural changes of the network; i.e., BDBA molecules and Fe atoms form an irregular pattern. In this process, the pristine Fe dimer motif is not preserved. Further, spherical features appear in close proximity to ligand molecules and Fe coordination centers (Figure 3). The size and shape of these protrusions are uniform (see the Supporting Information, section 1) and compatible with earlier reported observations of CO_2 molecules on metal surfaces.[41,42] The breaking of the network structure suggests a weakening of the established Fe−carboxylate coordination bonds when CO_2 molecules bind close to the coordination centers, as will be discussed below. The Ag surface alone can be ruled out to activate CO_2 via charge transfer from the substrate since CO_2 interacts only with surfaces more reactive than Ag, which is confirmed by the absence of any CO_2 related features on the bare Ag surface areas.[43,44] However, adsorbates on the Ag substrate may enhance the interaction with CO_2.[41] Hence, in the following, we will only consider CO_2 directly interacting with the components of the network. Since the pristine MOCN is thermally robust, which is a consequence of the appreciable strength of the coordination bonds (~1.3 eV per bond), according to our DFT calculations (see Table S1 in the Supporting Information) and in agreement with ref 45, we expect that the majority of Fe atoms is still engaged in coordination bonds to the carboxylate ligands in the collapsed network structure. This is supported by the STM data showing molecules pointing to a common center, however in motifs different from the pristine Fe dimer structure. We note that not all observed protrusions and features in the STM images of the collapsed structure could be unambiguously identified, and therefore, only clear appearances have been used in the detailed analysis.

Information on the energetics of the CO_2 adsorption can be gained from mass filtered temperature-induced desorption experiments. The data in Figure 4 reveal the release of CO_2 with a peak temperature of 190 K, which demonstrates a moderate binding of CO_2 within the collapsed network. The second dominant desorption peak associated with CO is also observed. Its magnitude is close to the one measured during the control experiment, and hence, excess CO desorbing from the sample cannot be confirmed (see also the Supporting Information, section 5). Moreover, the observed peak is very broad, which suggests a broad range of binding energies associated with various binding motives. In comparison, CO_2 does not adsorb on the more reactive Ag(110) surface at 100 K and desorbs at 130 K from an oxygen precovered Ag(110)

DOI: 10.1021/acs.jpcc.6b05582
J. Phys. Chem. C 2016, 120, 18622−18630

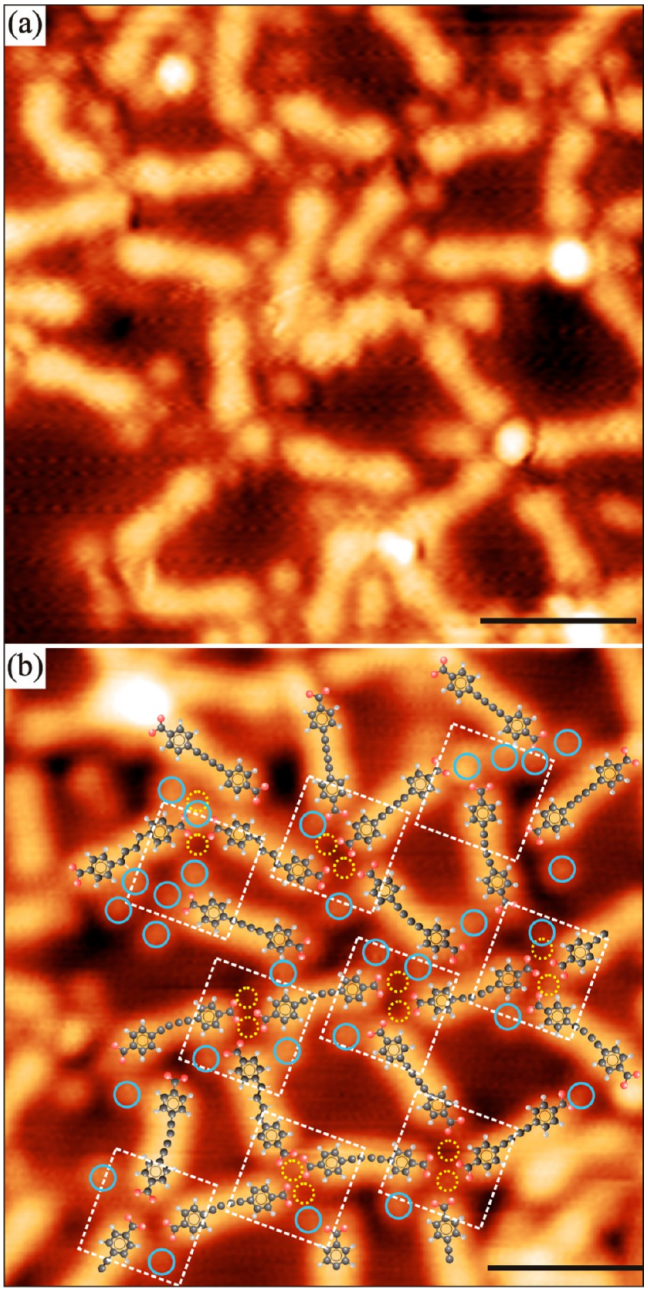

Figure 3. Representative STM images of the Fe-BDBA coordination network on Ag(001) after dosing 100 L of CO_2 at $T_{substrate}$ = 105 K and imaging at 5 K. In (b), the dashed white squares and dotted yellow circles mark the inferred original position of coordination centers and Fe atoms, respectively. The position of the spherical features which are assigned to CO_2 molecules is represented by blue circles. Acquisition parameters: +0.1 V, 1.0 nA. Scale bars: 2 nm.

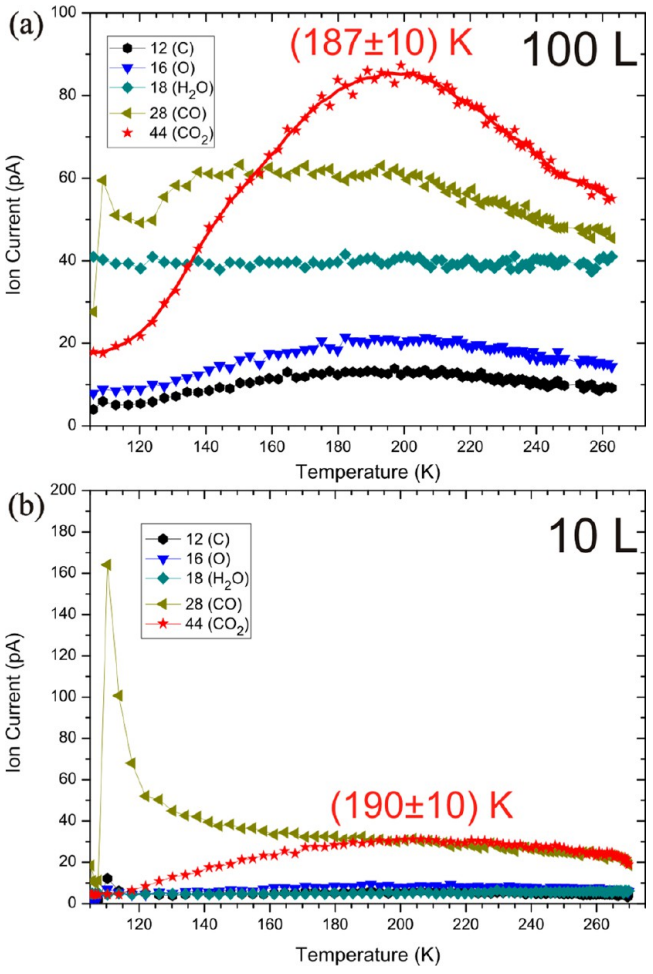

Figure 4. Mass filtered temperature induced desorption curves measured on samples with Fe-BDBA coordination networks dosed with (a) 100 L and (b) 10 L of CO_2. The mass of fragments (in amu) is given in the legend together with their chemical assignments. In addition to the CO_2 related peak, the peaks of C, O, and CO (excluding the initial peak) are also observed as a result of CO_2 molecule fragmentation in the mass spectrometer during the ionization process. The steep onset of CO desorption at about 105 K is ascribed to a burst from the starting filament and desorption from the precooled manipulator (adsorbed from residual CO atmosphere in UHV), which was also observed in the control experiments for a sample without CO_2 dosing. The given temperatures refer to the position of the CO_2 desorption peak.

substrate.[46] Only weak CO_2 physisorption is reported on unreconstructed low index Ag surfaces at temperatures much lower than 100 K. Preadsorbed oxygen on Ag was shown to enhance the reactivity, leading to the formation of carbonates or CO_2 chemisorption.[41,43,47,48] In our case, nearly all spherical features disappear upon annealing above room temperature. Hence, based on the STM and desorption data, we assign the spherical adsorbates to moderately bound CO_2 molecules. As shown in Figure 5, annealing the system at elevated temperatures (460 K) does not restore a full reticulation of the original square network structure, assuming the chemical identity in reference to pristine Fe-BDBA synthesis. Instead, network nodes coordinating to more than four molecules or triangular or larger cavities are observed. We assume that, during the annealing, the network is trapped in metastable bonding arrangements with considerable stability, which is ascribed in part to the ligand flexibility and formation of larger Fe clusters. Indeed, the formation of these thermodynamically trapped structures is avoided by the codeposition method of the original network structure.[31]

To trace the elementary changes caused by the incorporation of CO_2 to the Fe-BDBA networks and identify the additional features in the STM topographs, we used lower CO_2 doses of 1 and 10 L on the pristine Fe-BDBA network (Figure 6a–e). The overview image in Figure 6a shows a largely intact network with only a few well-separated structural changes within the network domains. At the periphery of the Fe-MOCN domains, bright

DOI: 10.1021/acs.jpcc.6b05582
J. Phys. Chem. C 2016, 120, 18622–18630

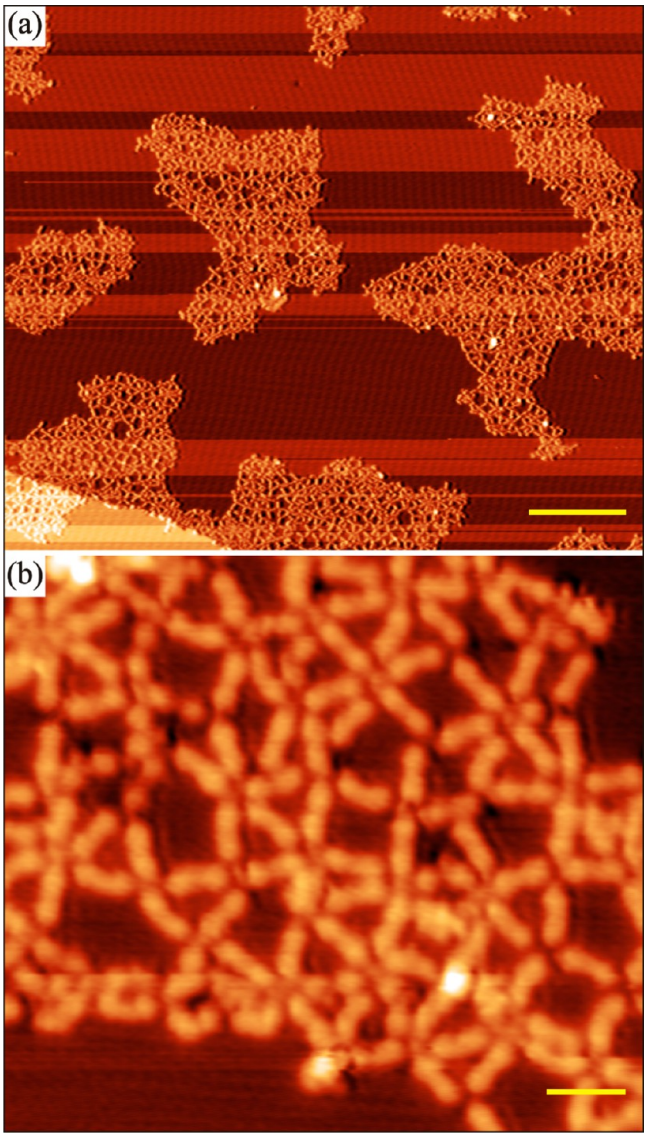

Figure 5. (a) Overview and (b) high-resolution images taken on samples dosed with 100 L of CO_2 at 105 K and subsequent annealing to 456 K for 5 min. The change of overall contrast in (a) is caused by changing tip conditions during scanning. Acquisition parameters: 5 K, 0.026 V, 1.0 nA. Scale bars: (a) 20 nm and (b) 2 nm.

features can be distinguished at almost all nodes or terminal carboxylate groups (Figure 6a,b), which we attribute to the immobilization of transient surface adsorbed CO_2 species at available binding sites (see below). Similar circular features are also observed within the network area, which are absent for the pristine structures. Besides their shape and apparent height, further evidence for the identity of the CO_2-adsorbates comes from low-temperature adsorption of CO_2 on the iron-free molecular phase of BDBA (see the Supporting Information, section 2), where similar-sized protrusions immerse into the pristine BDBA-chevron pattern. This observation also demonstrates the affinity of CO_2 to the carboxylate ligands adsorbed on the Ag surface.

During the structural changes, the BDBA ligands are either moved from their original position together with the Fe atoms or separated from them by inserted CO_2. In both cases, the Fe is released from the original coordination bonding and position on the surface. Hence, we look into the details of the

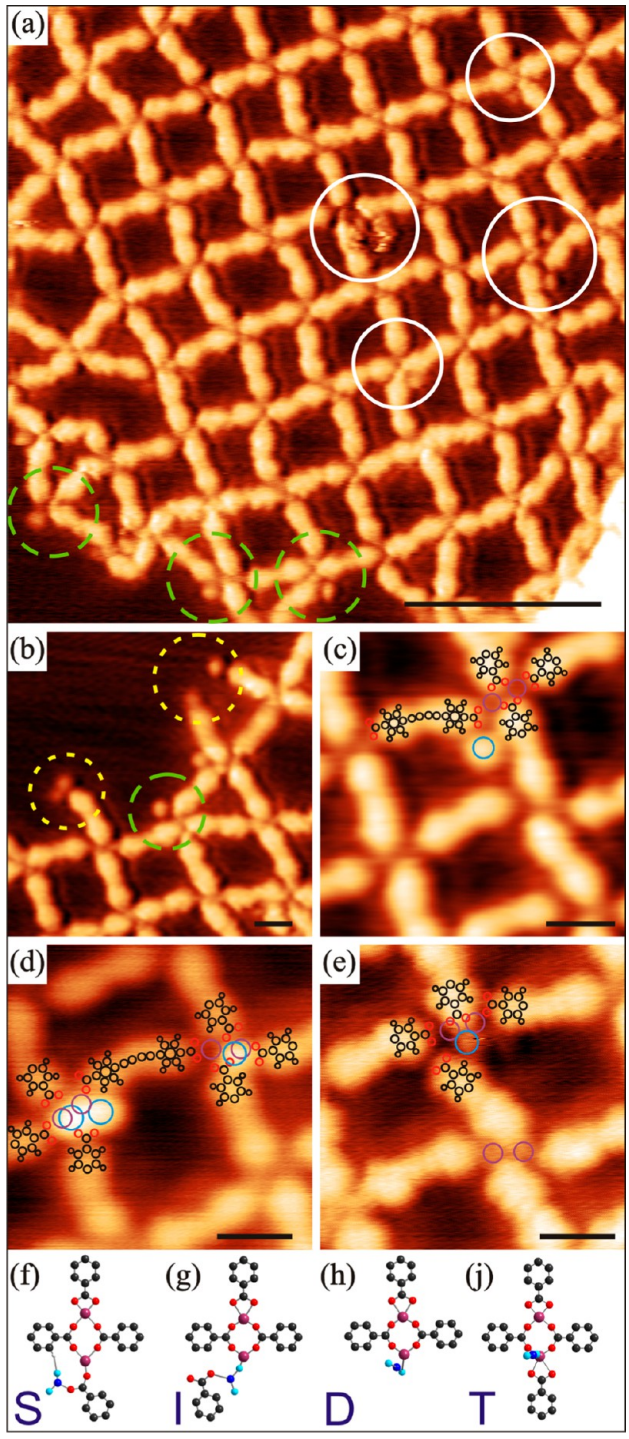

Figure 6. STM images of Fe-BDBA coordination networks on Ag(001) after dosing 10 L (a, b) and 1 L (c, d, e) of CO_2. White solid circles identify elementary events inside the network, green dashed circles mark CO_2 interaction with peripheral Fe centers, and yellow dotted circles highlight CO_2 binding to terminal carboxylate groups. In panels (c), (d), and (e), the BDBA molecules are highlighted with black (C and H atoms)/red (O atoms) contours, and the Fe atoms and CO_2 are marked by purple and blue circles, respectively. Schemes (f)−(j) depict our inferred guesses (S, I, D, and T) for the elementary binding modes of CO_2. Iron atoms are represented as purple circles, the phenyl-carboxylate part of BDBA is depicted by a black/red symbol, and CO_2 is portrayed in blue tones. In S, a hydrogen bond between CO_2 and the adjacent phenyl ring is indicated. Acquisition parameters: 5 K, 0.2 V, 1.0 nA (a, b), 0.4 V, 1.0 nA (d), and 0.4 V, 0.6 nA (c, e). Scale bars: 5 nm (a) and 1 nm (c, d, e).

DOI: 10.1021/acs.jpcc.6b05582
J. Phys. Chem. C 2016, 120, 18622−18630

arrangements and can recognize several characteristic structural motifs for both high and low CO_2 doses: (i) The most noticeable observation is the complete detachment of BDBA ligands from the coordination node for the high dose (Figure 3b). Apparently, the majority of these ligands displays CO_2 protrusions in the vicinity of their carboxylate groups. The estimated distance between the carboxylate oxygen and the center of the CO_2 protrusion is (0.28 ± 0.03) nm. (ii) In a second configuration (hereafter referred to as S), the BDBA carboxylate moiety coordinates with one oxygen atom to an iron atom, whereas the other oxygen atom is in close proximity to a CO_2 molecule (Figure 6c,f). In this case, we find an oxygen−CO_2 distance of (0.29 ± 0.01) nm. (iii) Another arrangement involves a CO_2 protrusion in close proximity of a Fe center where the formerly bonded BDBA ligand is displaced from its original position and no longer coordinates to the Fe centers; i.e., the CO_2 is inserted into the Fe−carboxylate bond (Figure 6e,g; further noted as I). This is observed for both bridging and axial ligands with preference for the latter. (iv) CO_2 is found at an open in-plane coordination position of an Fe coordination center, i.e., without further connection to a nearby BDBA ligand (structure D in the following). This motif is observed mainly at the network periphery or at the position of a completely released BDBA ligand; this is documented in Figures 3b and 6a,h. (v) A protrusion is also found on top of an Fe dimer (structure T). In this case, one bridging ligand is slightly shifted/rotated in comparison to intact coordination nodes (Figure 6d,j). Generally, there is a low amount of features S, I, and T observed within the intact network after the low CO_2 dosing (1 or 10 L). These occur preferentially at the network periphery or in the vicinity of structural defects within the network.

The observed structural distortions after CO_2 dosing shown in the STM images of Figures 3 and 6 can be tentatively assigned to the ambivalent reactivity of CO_2—electrophilic carbon atom and nucleophilic oxygen atoms. Hence, in principle, two pathways of attack seem feasible: either an electrophilic attack of the carbon atom of CO_2 to one of the electron rich oxygen atoms of the carboxylate groups of BDBA (Figure 6c,f) (see also the Supporting Information, section 2, for BDBA molecular phase) or a nucleophilic attack of the oxygen atoms of CO_2 to the coordinatively unsaturated Fe atoms or the adjacent hydrogen atoms of the BDBA ligand (Figure 6d,e,j). In the following, we will use DFT calculations to elucidate the different modes of CO_2 binding. The structural motifs recognized in the STM images and rationalized by the proposed tentative models (S, I, D, and T) in Figure 6f−j have been used as initial geometries for optimization in our DFT calculations of CO_2 adsorption on the reduced Fe-carboxylate models shown in Figure 2c. The results of these calculations are displayed in Figure 7a,c,e, corresponding to the cases S, I, and D, respectively, for which we find stable binding geometries after structural relaxation. Their corresponding simulated STM appearances are shown in Figure 7b,d,f. In the S structure, the oxygen−CO_2 distance of 0.3 nm appears in good agreement with the experimental value of 0.29 ± 0.01 nm. However, the CO_2 carbon atom adopts a linear O−C−O configuration, evidencing very low charge transfer and weak binding. Although just represented in case I, many structures with CO_2 insertion in the Fe−carboxylate bond can be optimized for both bridging and axial ligands. Concerning the D structure that appears frequently at the network periphery with CO_2 directly binding in-plane with the Fe dimer, it has been

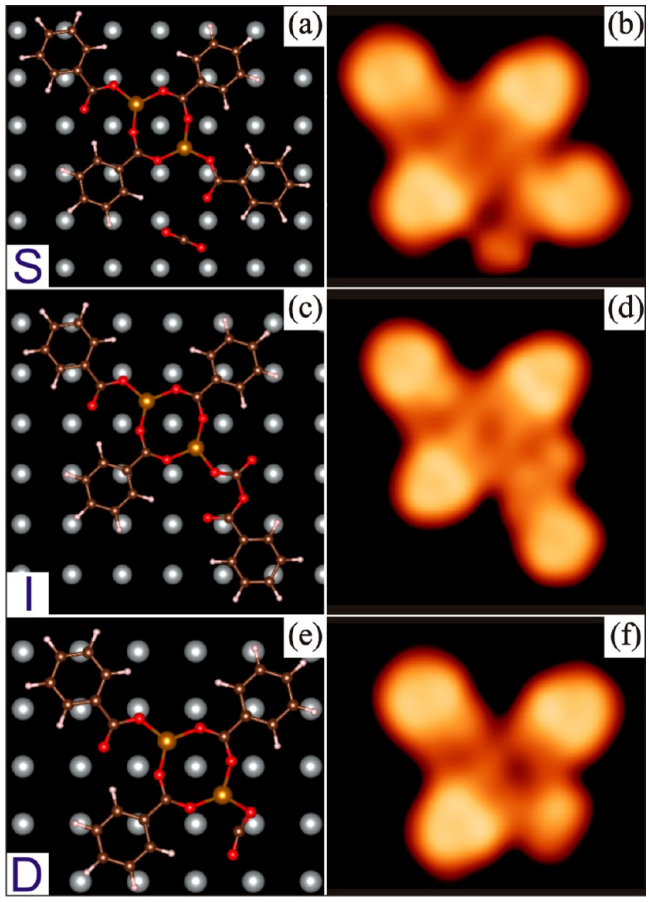

Figure 7. Panels (a), (c), and (e) are optimized structures from DFT calculations for the adsorption of CO_2 on the Fe-BDBA coordination network represented with a ball-and-stick model, corresponding to the initial guesses S, I, and D. Their corresponding calculated molecular appearances are shown in panels (b), (d), and (f).

optimized similarly to its initial guess and could also be obtained in various, though similar, structures. It is interesting to note that the structure I indeed shows clearly a tilted O−C−O geometry, a strong indication for CO_2 activation.

Finally, although we reproduced the experimentally inferred structural guesses for the models S, I, and D in the DFT calculations, we did not find a direct stable bonding configuration of CO_2 on top of the Fe dimer corresponding to case T in Figure 6j. The Fe centers are electron depleted in the carboxylate environment. According to a Bader charge analysis, a total valence electron number is 6.79, which is in agreement with reports for similar systems.[23,49] To chemically bind CO_2 leading to the molecular $CO_2^{\delta-}$ anion with tilted O−C−O geometry, electrons must be transferred to the adsorbed CO_2, which, in this scenario, could consequently be charge-compensated by oxidation of the Fe atoms. However, such oxidation would cause strong structural changes of the network and certainly the disruption of the dimeric structure. Although a previous report for O_2 adsorbates on top of an Fe-carboxylate complex assembled on a Cu surface shows that electrons can be transferred to O_2 from the surface beneath the complex,[23] this appears less likely in the case of the more noble Ag substrate. We conclude that Fe is hindered to reach a higher oxidation state in its given chemical environment of the models in Figure 2b,c on the Ag surface, thus impeding the top binding of CO_2 in the theoretical models.

DOI: 10.1021/acs.jpcc.6b05582
J. Phys. Chem. C 2016, 120, 18622−18630

An energetic analysis based on our DFT calculations (see Tables S1 and S2 in sections 7 and 9 of the Supporting Information) reveals a weakening of the Fe−O bonds due to CO_2 adsorption in structure I up to 200 meV. The binding of CO_2 near a free carboxylate oxygen atom as in structure S is relatively weak (a few tenths of eV), and thus, we do not expect major changes for the network structure. These figures could hardly justify a network collapse as experimentally observed. Since the vast majority of the binding events at low coverage was observed at the network periphery with irregular coordination centers or in the vicinity of defective structural nodes, we performed calculations for more open network structures, i.e., with an artificially increased Fe−carboxylate bond length as a model to test the reactivity at the irregular nodes (see the Supporting Information, section 8). The calculations show that the CO_2 molecule has a more direct access to the Fe dimer with a significant interaction between CO_2 and Fe that eventually leads even to dissociation of CO_2 in the calculations. Dissociative adsorption of a few CO_2 molecules might appear at high CO_2 exposure. For these reasons, we have also theoretically and experimentally investigated the binding of CO on the pristine structure in Figure 2c. The DFT calculations show that CO interacts generally stronger than CO_2 and also binds stably on top of an iron atom at the pristine coordination nodes (see the Supporting Information, section 9). We find a stronger weakening (close to 1 eV in some cases) of the Fe−carboxylate bonds for CO binding to the Fe centers. This is consistent with the experimental observation of the disruption of the network structure after CO dosing (see the Supporting Information, section 3). Considering the observed impact of CO_2 on the network structure, we argue that, due to the structural variety of Fe network nodes found in the experiments in comparison to the ideal and structurally relaxed theoretical model, CO_2 molecules react first at the Fe centers of the irregular nodes (that are more reactive) in the network, producing a local distortion that propagates as CO_2 exposure increases. The full dissociation of CO_2 in the theoretical models does not necessarily occur in the proposed reaction pathway as the Fe−carboxylate bond progressively opens during the CO_2 adsorption at a defective site and a concerted movement of CO_2 and ligands is expected to lead to the experimentally observed energetically trapped intermediate configurations with moderate binding strengths. Note that these rearrangements necessarily occur in the real structure due to the connection of the ligands to different nodes and the simultaneous optimization of several coordination bonds at both ends of the ligands, which cannot be captured in the theoretical models.

From the DFT calculations, we cannot trace back the collapse of the MOCN to a single CO_2 adsorption configuration. The direct bonding to the Fe centers likely appears as initial states where we can distinguish two distinct sites: One case is CO_2 attack on top of Fe centers, i.e., model T. In the other case, one oxygen atom of the CO_2 molecule is involved in a direct in-plane covalent bond with an iron atom after complete detachment of a BDBA ligand (structure D) or insertion within the coordination node (structure I). This hints that coordination nodes with 3-fold coordinated Fe centers, i.e., monodentate binding of axial ligands, are more susceptible for this reaction path due to the more open area around the Fe center. The side attack of CO_2 in the more open coordination nodes of the real network could be more relevant than binding on top of Fe centers. On the other hand, for CO_2 binding on top of the Fe center, regardless if dissociative adsorption occurs or not, a concerted rearrangement of CO_2 and ligand might enable the insertion of CO_2 into the M−O bond. Hence, we propose that, under these assumptions, the network structure collapses starting by the more defective nodes with more open coordination Fe centers.

CONCLUSIONS

In conclusion, we investigated the reactivity of a model system with coordinatively unsaturated metal centers at surfaces toward CO_2 at low temperatures and low CO_2 partial pressures. CO_2 readily reacts with the components of the metal−organic network and strongly modifies the present coordination environment, which, in this extent, is unexpected and surprising. STM data at the single molecule level reveal characteristic binding motifs of CO_2 with both the Fe centers and the carboxylate moieties of the ligands, which ultimately lead to the collapse of the network structure. On the basis of STM data, several binding configurations are proposed and rationalized with DFT calculations. The theoretical analysis of an idealized model shows that the associated bond energy changes are not sufficient to explain the observed structural rearrangements. We propose that the binding of CO_2 on distorted or irregular Fe centers can lead to significant interaction energies, accompanied by irreversible structural rearrangements of the original network structure. The initial local disruption of the network structure can then propagate through the entire surface structure at higher CO_2 dosing levels. The studied model system provides insights in the local interactions of CO_2 with the components of a metal−organic network, which showed a variety of binding modes and an intricate mechanism for the weakening of the Fe−carboxylate coordination bonds of the pristine network. Further experimental and theoretical efforts aim to explore the details of the reaction mechanism and the chemical state of the potentially activated CO_2 molecules. We envision that the exploration of metal−organic coordination structures at the surface studied at the single molecule level may reveal further unprecedented processes and reaction pathways that are relevant for the advancement of real catalytic systems.

ASSOCIATED CONTENT

Supporting Information

The Supporting Information is available free of charge on the ACS Publications website at DOI: 10.1021/acs.jpcc.6b05582.

Additional information is provided regarding the STM traces of Fe and CO_2 adsorbates, CO_2 adsorption on the molecular network, STM images after CO dosing, impurity analysis for the adsorption experiments, additional mass spectra, DFT structure and energetics of the networks, and the DFT analysis of the structure and energetics for CO_2 and CO binding on the networks (PDF)

AUTHOR INFORMATION

Corresponding Authors

*E-mail: cechal@fme.vutbr.cz. Phone: +420 541 142 810 (J.Č.).

*E-mail: sebastian.stepanow@mat.ethz.ch. Phone: +41 44 633 07 41 (S.S.).

DOI: 10.1021/acs.jpcc.6b05582
J. Phys. Chem. C 2016, 120, 18622−18630

Present Address

◆Department of Chemistry, University of California, Berkeley, California 94720, United States.

Author Contributions

The manuscript was written through contributions of all authors. All authors have given approval to the final version of the manuscript.

Notes

The authors declare no competing financial interest.

■ ACKNOWLEDGMENTS

This work was supported by the Baden-Württemberg Stiftung and SFB TR 88 "3MET". J.Č. acknowledges the funding provided by Marie Curie IEF within the seventh FP (AdaptNano, Project No. 251930) and the MEYS, project No. LQ1601 (CEITEC 2020). R.P. and A.A. are thankful for the partial financial support by MINECO (grant# FIS2013-48286-C2-8752-P), UPV/EHU and Eusko Jaurlaritza (grant# IT-756-13).

■ REFERENCES

(1) Chu, S.; Majumdar, A. Opportunities and challenges for a sustainable energy future. *Nature* **2012**, *488*, 294−303.

(2) Cokoja, M.; Bruckmeier, C.; Rieger, B.; Herrmann, W. A.; Kuhn, F. E. Transformation of carbon dioxide with homogeneous transition-metal catalysts: A molecular solution to a global challenge? *Angew. Chem., Int. Ed.* **2011**, *50*, 8510−8537.

(3) Drees, M.; Cokoja, M.; Kuhn, F. E. Recycling CO_2? Computational considerations of the activation of CO_2 with homogeneous transition metal catalysts. *ChemCatChem* **2012**, *4*, 1703−1712.

(4) Liu, Q.; Wu, L.; Jackstell, R.; Beller, M. Using carbon dioxide as a building block in organic synthesis. *Nat. Commun.* **2015**, *6*, 5933.

(5) Aresta, M.; van Eldik, R., Eds. *CO_2 Chemistry: Advances in Inorganic Chemistry*; Elsevier Academic Press: San Diego, CA, 2014; Vol. *66*.

(6) Dubois, M. R.; Dubois, D. L. Development of molecular electrocatalysts for CO_2 reduction and H_2 production/oxidation. *Acc. Chem. Res.* **2009**, *42*, 1974−1982.

(7) Reda, T.; Plugge, C. M.; Abram, N. J.; Hirst, J. Reversible interconversion of carbon dioxide and formate by an electroactive enzyme. *Proc. Natl. Acad. Sci. U. S. A.* **2008**, *105*, 10654−10658.

(8) Xie, Y.; Wang, T.-T.; Liu, X.-H.; Zou, K.; Deng, W.-Q. Capture and conversion of CO_2 at ambient conditions by a conjugated microporous polymer. *Nat. Commun.* **2013**, *4*, 1960.

(9) Toda, Y.; Hirayama, H.; Kuganathan, N.; Torrisi, A.; Sushko, P. V.; Hosono, H. Activation and splitting of carbon dioxide on the surface of an inorganic electride material. *Nat. Commun.* **2013**, *4*, 2378.

(10) O'Keeffe, M.; Yaghi, O. M. Deconstructing the crystal structures of metal−organic frameworks and related materials into their underlying nets. *Chem. Rev.* **2012**, *112*, 675−702.

(11) Meek, S. T.; Greathouse, J. A.; Allendorf, M. D. Metal-organic frameworks: a rapidly growing class of versatile nanoporous materials. *Adv. Mater.* **2011**, *23*, 249−267.

(12) Park, J.; Kim, H.; Han, S. S.; Jung, Y. Tuning metal−organic frameworks with open-metal sites and its origin for enhancing CO_2 affinity by metal substitution. *J. Phys. Chem. Lett.* **2012**, *3*, 826−829.

(13) Sumida, K.; Rogow, D. L.; Mason, J. A.; McDonald, T. M.; Bloch, E. D.; Herm, Z. R.; Bae, T.-H.; Long, J. R. Carbon dioxide capture in metal−organic frameworks. *Chem. Rev.* **2012**, *112*, 724−781.

(14) Burtch, N. C.; Jasuja, H.; Dubbeldam, D.; Walton, K. S. Molecular-level insight into Unusual low pressure CO_2 affinity in pillared metal−organic frameworks. *J. Am. Chem. Soc.* **2013**, *135*, 7172−7180.

(15) Liao, P.-Q.; Zhou, D.-D.; Zhu, A.-X.; Jiang, L.; Lin, R.-B.; Zhang, J.-P.; Chen, X.-M. Strong and dynamic CO_2 sorption in a flexible porous framework possessing guest chelating claws. *J. Am. Chem. Soc.* **2012**, *134*, 17380−17383.

(16) Poloni, R.; Lee, K.; Berger, R. F.; Smit, B.; Neaton, J. B. Understanding trends in CO_2 adsorption in metal−organic frameworks with open-metal sites. *J. Phys. Chem. Lett.* **2014**, *5*, 861−865.

(17) Yoon, M.; Srirambalaji, R.; Kim, K. Homochiral metal−organic frameworks for asymmetric heterogeneous catalysis. *Chem. Rev.* **2012**, *112*, 1196−1231.

(18) Kornienko, N.; Zhao, Y.; Kley, C. S.; Zhu, C.; Kim, D.; Lin, S.; Chang, C. J.; Yaghi, O. M.; Yang, P. Metal−organic frameworks for electrocatalytic reduction of carbon dioxide. *J. Am. Chem. Soc.* **2015**, *137*, 14129−14135.

(19) Barth, J. V.; Costantini, G.; Kern, K. Engineering atomic and molecular nanostructures at surfaces. *Nature* **2005**, *437*, 671−679.

(20) Elemans, J.A.A.W; Lei, S.; De Feyter, S. Molecular and supramolecular networks on surfaces: from two-dimensional crystal engineering to reactivity. *Angew. Chem., Int. Ed.* **2009**, *48*, 7298−7332.

(21) Barth, J. V. Fresh perspectives for surface coordination chemistry. *Surf. Sci.* **2009**, *603*, 1533−1541.

(22) Gutzler, R.; Stepanow, S.; Grumelli, D.; Lingenfelder, M.; Kern, K. Mimicking enzymatic active sites on surfaces for energy conversion chemistry. *Acc. Chem. Res.* **2015**, *48*, 2132−2139.

(23) Fabris, S.; Stepanow, S.; Lin, N.; Gambardella, P.; Dmitriev, A.; Honolka, J.; Baroni, S.; Kern, K. Oxygen dissociation by concerted action of di-iron centers in metal−organic coordination networks at surfaces: modeling non-heme iron enzymes. *Nano Lett.* **2011**, *11*, 5414−5420.

(24) Grumelli, D.; Wurster, B.; Stepanow, S.; Kern, K. Bio-inspired nanocatalysts for the oxygen reduction reaction. *Nat. Commun.* **2013**, *4*, 2904.

(25) Clough, A. J.; Yoo, J. W.; Mecklenburg, M. H.; Marinescu, S. C. Two-dimensional metal−organic surfaces for efficient hydrogen evolution from water. *J. Am. Chem. Soc.* **2015**, *137*, 118−121.

(26) Wurster, B.; Grumelli, D.; Hötger, D.; Gutzler, R.; Kern, K. Driving the oxygen evolution reaction by nonlinear cooperativity in bimetallic coordination catalysts. *J. Am. Chem. Soc.* **2016**, *138*, 3623−3626.

(27) Feng, M.; Sun, H.; Zhao, J.; Petek, H. Self-catalyzed carbon dioxide adsorption by metal-organic chains on gold surfaces. *ACS Nano* **2014**, *8*, 8644−8652.

(28) Feng, M.; Petek, H.; Shi, Y.; Sun, H.; Zhao, J.; Calaza, F.; Sterrer, M.; Freund, H.-J. Cooperative chemisorption-induced physisorption of CO_2 molecules by metal-organic chains. *ACS Nano* **2015**, *9*, 12124−12136.

(29) Berland, K.; Hyldgaard, P. Exchange functional that tests the robustness of the plasmon description of the van der Waals density functionals. *Phys. Rev. B: Condens. Matter Mater. Phys.* **2014**, *89*, 035412.

(30) Björkman, T. Testing several recent van der Waals density functionals for layered structures. *J. Chem. Phys.* **2014**, *141*, 074708.

(31) Kley, C. S.; Cechal, J.; Kumagai, T.; Schramm, F.; Ruben, M.; Stepanow, S.; Kern, K. Highly adaptable two-dimensional metal−organic coordination networks on metal surfaces. *J. Am. Chem. Soc.* **2012**, *134*, 6072−6075.

(32) Cechal, J.; Kley, C. S.; Kumagai, T.; Schramm, F.; Ruben, M.; Stepanow, S.; Kern, K. Functionalization of open two-dimensional metal−organic templates through the selective incorporation of metal atoms. *J. Phys. Chem. C* **2013**, *117*, 8871−8877.

(33) Cechal, J.; Kley, C. S.; Kumagai, T.; Schramm, F.; Ruben, M.; Stepanow, S.; Kern, K. Convergent and divergent two-dimensional coordination networks formed through substrate activated or quenched alkynyl ligation. *Chem. Commun.* **2014**, *50*, 9973−9976.

(34) Kresse, G.; Hafner, J. Ab initio molecular-dynamics simulation of the liquid-metal-amorphous-semiconductor transition in germanium. *Phys. Rev. B: Condens. Matter Mater. Phys.* **1994**, *49*, 14251−14269.

(35) Kresse, G.; Furthmuller, J. Efficient iterative schemes for ab initio total-energy calculations using a plane-wave basis set. *Phys. Rev. B: Condens. Matter Mater. Phys.* **1996**, *54*, 11169−1118.

DOI: 10.1021/acs.jpcc.6b05582
J. Phys. Chem. C 2016, 120, 18622−18630

(36) González-Moreno, R.; Garcia-Lekue, A.; Arnau, A.; Trelka, M.; Gallego, J. M.; Otero, R.; Verdini, A.; Sánchez-Sánchez, C.; de Andrés, P. L.; Martín-Gago, J. A.; et al. Role of the anchored groups in the bonding and self-organization of macrocycles: carboxylic versus pyrrole groups. *J. Phys. Chem. C* **2013**, *117*, 7661−7668.
(37) Blöchl, P. E. Projector augmented-wave method. *Phys. Rev. B: Condens. Matter Mater. Phys.* **1994**, *50*, 17953−17979.
(38) Perdew, J. P.; Burke, K.; Ernzerhof, M. Generalized gradient approximation made simple. *Phys. Rev. Lett.* **1996**, *77*, 3865.
(39) Tersoff, J.; Hamann, D. R. Theory and application for the scanning tunneling microscope. *Phys. Rev. Lett.* **1983**, *50*, 1998−2001.
(40) Seitsonen, A. P.; Lingenfelder, M.; Spillmann, H.; Dmitriev, A.; Stepanow, S.; Lin, N.; Kern, K.; Barth, J. V. Density functional theory analysis of carboxylate-bridged diiron units in two-dimensional metal−organic grids. *J. Am. Chem. Soc.* **2006**, *128*, 5634−5635.
(41) Hsieh, M.-F.; Li, H.-D.; Lin, D.-S.; Morgenstern, K. Formation, binding, and stability of O-Ag-CO_2-Ag-O compounds on Ag(100) investigated by low temperature scanning tunneling microscopy and manipulation. *J. Phys. Chem. C* **2010**, *114*, 14173−14179.
(42) Lee, J.; Sorescu, D. C.; Deng, X. Electron-induced dissociation of CO_2 on TiO_2(110). *J. Am. Chem. Soc.* **2011**, *133*, 10066−10069.
(43) Burghaus, U. Surface chemistry of CO_2 − adsorption of carbon dioxide on clean surfaces at ultrahigh vacuum. *Prog. Surf. Sci.* **2014**, *89*, 161−217.
(44) Liu, C.; Cundari, T. R.; Wilson, A. K. CO_2 reduction on transition metal (Fe, Co, Ni, and Cu) surfaces: in comparison with homogeneous catalysis. *J. Phys. Chem. C* **2012**, *116*, 5681−5688.
(45) Clair, S.; Pons, S.; Fabris, S.; Baroni, S.; Brune, H.; Kern, K.; Barth, J. V. Monitoring two-dimensional coordination reactions: directed assembly of Co−terephthalate nanosystems on Au(111). *J. Phys. Chem. B* **2006**, *110*, 5627−5632.
(46) Stuve, E. M.; Madix, R. J.; Sexton, B. A. An EELS study of CO_2 and CO_3 adsorbed on oxygen covered Ag(110). *Chem. Phys. Lett.* **1982**, *89*, 48−53.
(47) Burghaus, U.; Vattuone, L.; Gambardella, P.; Rocca, M. HREELS study of CO oxidation on Ag(001) by O_2 or O. *Surf. Sci.* **1997**, *374*, 1−8.
(48) Guo, X.-C.; Madix, R. J. CO_2 + O on Ag(110): stoichiometry of carbonate formation, reactivity of carbonate with CO, and reconstruction-stabilized chemisorption of CO_2. *J. Phys. Chem. B* **2001**, *105*, 3878−3885.
(49) Gambardella, P.; Stepanow, S.; Dmitriev, A.; Honolka, J.; de Groot, F. M. F.; Lingenfelder, M.; Gupta, S. S.; Sarma, D. D.; Bencok, P.; Stanescu, S.; et al. Supramolecular control of the magnetic anisotropy in two-dimensional high-spin Fe arrays at a metal interface. *Nat. Mater.* **2009**, *8*, 189−193.

DOI: 10.1021/acs.jpcc.6b05582
J. Phys. Chem. C 2016, 120, 18622−18630